Precambrian Research 304 (2018) 88–98

Contents lists available at ScienceDirect

Precambrian Research

journal homepage: www.elsevier.com/locate/precamres

Cellular taphonomy of well-preserved Gaoyuzhuang microfossils: A window into the preservation of ancient cyanobacteria

Zixiao Guo[a,b], Xiaotong Peng[a,*], Andrew D. Czaja[c], Shun Chen[a], Kaiwen Ta[a]

[a] Deep Sea Science Division, Institute of Deep Sea Science and Engineering, Chinese Academy of Sciences, Sanya 572000, China
[b] University of Chinese Academy of Sciences, Beijing 100049, China
[c] Department of Geology, University of Cincinnati, PO Box 210013, Cincinnati, OH 45221-0013, USA

ARTICLE INFO

Keywords:
Gaoyuzhuang Formation
Microfossil
Cyanobacteria
Taphonomy
Morphological alteration
Molecular structure

ABSTRACT

The ~1500 Ma Gaoyuzhuang microfossils, a representative Mesoproterozoic cyanobacteria assemblage, are crucial for understanding and searching for early Precambrian life on Earth. The cellular taphonomy of fossils in this assemblage is poorly known, however. Here we combined *in situ* microscopic and microanalytical techniques to study the detailed taphonomy of these microfossils. Light microscopy (LM), scanning electron microscopy (SEM) and transmission electron microscopy (TEM) observations show that Gaoyuzhuang microfossils are mainly preserved in black chert layers and that silica particles can be found within fossilized cell walls and sheaths. Raman spectra show the characteristic first-order bands (at ~1350 and ~1605 cm^{-1}) of carbonaceous material comprising microfossils, indicating that they have experienced peak temperatures of ~215 to 308 °C. Raman maps show the spatial distribution of the carbonaceous matter as well as that of the silica matrix, consistent with nano-scale secondary ion mass spectrometry (NanoSIMS) analyses. Variations in ^{13}C versus ^{12}C and ^{34}S versus ^{32}S within individual microfossils are likely the result of original differences in the isotopic compositions of cellular components. Confocal laser scanning microscopy (CLSM) analyses provide fluorescence-based 2-D and 3-D images of the cellular components of such microfossils at high spatial resolution. The micro-scale chemical, isotopic and structural heterogeneities together with the subcellular morphological features support the preferential preservation of cyanobacterial cell walls and sheaths over cell contents in Precambrian chert. We proposed a potential taphonomic model, perhaps responsible for the high fidelity of preservation, for such microfossils permineralized in Precambrian rocks. The integrated approach has potential for deciphering the enigmatic nature of Mesoproterozoic microorganisms preserved in stromatolitic cherts, with significant implications for microbial preservation in the geological record.

1. Introduction

Cyanobacteria are a dominant, long-ranging and successful group of prokaryotic organisms, which are organically preserved in the geological record of most of Earth's history, possibly dating back 3500 million years (Ma) ago although relaxed molecular clocks suggest cyanobacteria originated about 2500–2600 Ma ago (Schopf, 1993, 2002; Schopf and Kudryavtsev, 2012; Shih et al., 2017). For more than half a century, such microfossils have been found in ancient marine and terrestrial aquatic environments from around the world (Barghoorn and Tyler, 1965; Schopf, 1968, 1993; Licari et al., 1969; Schopf et al., 1973, 2005, 2015; Hofmann, 1976; Schopf and Packer, 1987; Ogurtsova and Sergeev, 1987; Sergeev, 1994; Altermann and Schopf, 1995; Xu and Awramik, 2002; Sergeev and Schopf, 2010). These cyanobacteria would have played a key role in increasing the amount of oxygen in the oceans and atmosphere on the Earth (House et al., 2000; Williford et al., 2013; Peng et al., 2016; Soo et al., 2017).

The ~1500 Ma Gaoyuzhuang Formation, exposed on the southern mountain of Pangjiapu, Hebei Province, China, contains some of the best-preserved Proterozoic filamentous and coccoidal microfossils (Zhang, 1981; Schopf et al., 1984, 2005; Peng et al., 2016). These microfossils were originally assigned to cyanobacteria on the basis of cell morphology, size, colonial patterns and by comparison with modern analogues (Zhang, 1981), and were subsequently studied in order to address questions about their paleobiology, paleoecology, paleoenvironment and thermal maturity (Schopf et al., 1984, 2005; Seong-Joo and Golubic, 1999; Golubic and Seong-Joo, 1999; Xu and Awramik, 2002). Fossils from this unit were more recently investigated and shown to have typical carbon isotope values ($\delta^{13}C$) for chroococcacean cyanobacteria, which implies oxygenic photosynthesis existed in the

* Corresponding author.
E-mail address: xtpeng@idsse.ac.cn (X. Peng).

https://doi.org/10.1016/j.precamres.2017.11.007
Received 28 May 2017; Received in revised form 10 November 2017; Accepted 15 November 2017
Available online 16 November 2017
0301-9268/

Mesoproterozoic anoxic ocean, and confirmed a linear correlation between average *in situ* $\delta^{13}C_{org}$ of microfossils and $\delta^{13}C_{carb}$ of coeval carbonates (Peng et al., 2016). Some of the prominent species of early cyanobacteria in the Gaoyuzhuang microfossils assemblage include *Eosynechococcus medius, Glenobotrydion aenigmatis*, *Nanococcus vulgaris*, and *Palaeoanacystis vulgaris* (Zhang, 1981; Schopf et al., 2005; Peng et al., 2016). The high degree of morphological preservation of this microfossil assemblage assures its use as a baseline with which to study older assemblages preserved in Precambrian rocks.

For a better understanding of cyanobacterial preservation in the geological record, we conducted a cellular taphonomic investigation of Gaoyuzhuang microfossils. The combined *in situ* techniques of FIB-based imaging, NanoSIMS (nano-scale secondary ion mass spectrometry), Raman spectroscopy, and CLSM (confocal laser scanning microscopy) were used to characterize Gaoyuzhuang microfossils in three dimensions and at submicron spatial resolution, to identify: 1) the ultrastructure of such rock-embedded microfossils; 2) the molecular–chemical characteristics of both the well-preserved microfossils and their embedding minerals; and 3) the organismal morphology of such rock-embedded microfossils. Here, we report three-dimensional organismal morphology, chemical and isotopic composition characteristics for Gaoyuzhuang microfossils and propose a potential taphonomic model for such microfossils. Due to the ancient depositional age and excellent preservation, the Gaoyuzhuang Formation represents a rare window into the preservation of cyanobacteria on the early Earth.

2. Materials and methods

2.1. Sampling location and sample descriptions

Microfossils studied here come from cherty stratiform stromatolites of the ~1500 Ma Gaoyuzhuang Formation, southern mountain of Pangjiapu, Hebei Province, China (Peng et al., 2016). Fig. 1 shows the sampling location and field photos of the cherty stromatolites, characterized by alternating black organic-rich chert bands and white carbonate bands at the centimeter to millimeter scales. The local geology and stratigraphy of the study area has been described in detail elsewhere (Zhang, 1981; Peng et al., 2016). All microfossils were analyzed in ~100-μm-thick polished thin sections cut from rock samples perpendicular to bedding. The samples and their geological background information are summarized in Table 1. This study concentrated on the spheroidal or ellipsoidal cells of this unit in order to provide new insights into cellular taphonomy of well-preserved Gaoyuzhuang microfossils, potentially deciphering cyanobacterial preservation in the geological record.

2.2. Analytical methods

Individual microfossils were observed within polished thin sections using a Leica DM4500P Polarizing Light Microscope. Specimens at the surface of thin sections were selected and photographed in transmitted and reflected light, with which sketch maps were constructed to identify each of the regions of interest (ROIs) for SEM (scanning electron microscopy), TEM (transmission electron microscopy), NanoSIMS, Raman spectroscopy and CLSM.

All microfossils at the surface of the polished thin section were examined with a Philips XL-30 scanning electron microscope equipped with an EDAX energy dispersive X-ray spectrometer and analytical software in Tongji University, China. The SEM was operated at 15 kV with a working distance of 10 mm to provide optimal imaging and minimize charging and sample damage in the backscattered electron (BSE) imaging mode. An accelerating voltage of 20 kV was used for the X-ray analysis to obtain sufficient X-ray counts (Peng et al., 2013, 2016). To prepare TEM lamellae from the polished thin section, dual-beam focused ion beam (FIB) milling was performed with the FEI Helios 600i FIB at the Analysis and Research Center, Shanghai University, China. During FIB milling, the selected microfossils were located and monitored within the dual-beam FIB by using electron beam imaging. TEM data were obtained using a JEM-2100F field emission electron microscope operating at 200 kV in the National Engineering Research Center for Nanotechnology (NERCN), China.

Elemental mapping was performed on the polished thin sections using a Cameca NanoSIMS 50L (CAMECA, Paris, France) at the Institute of Geology and Geophysics, Chinese Academy of Sciences, following the procedure described in Peng et al. (2016). Using a focused primary beam of cesium (Cs+) with an ~2.5 pA intensity, negatively charged secondary ions ($^{12}C^-$, $^{13}C^-$, $^{12}C^{14}N^-$, $^{32}S^-$, $^{34}S^-$, $^{55}Mn^{16}O^-$, and $^{56}Fe^{16}O_2^-$) were sputtered from each ROIs and collected

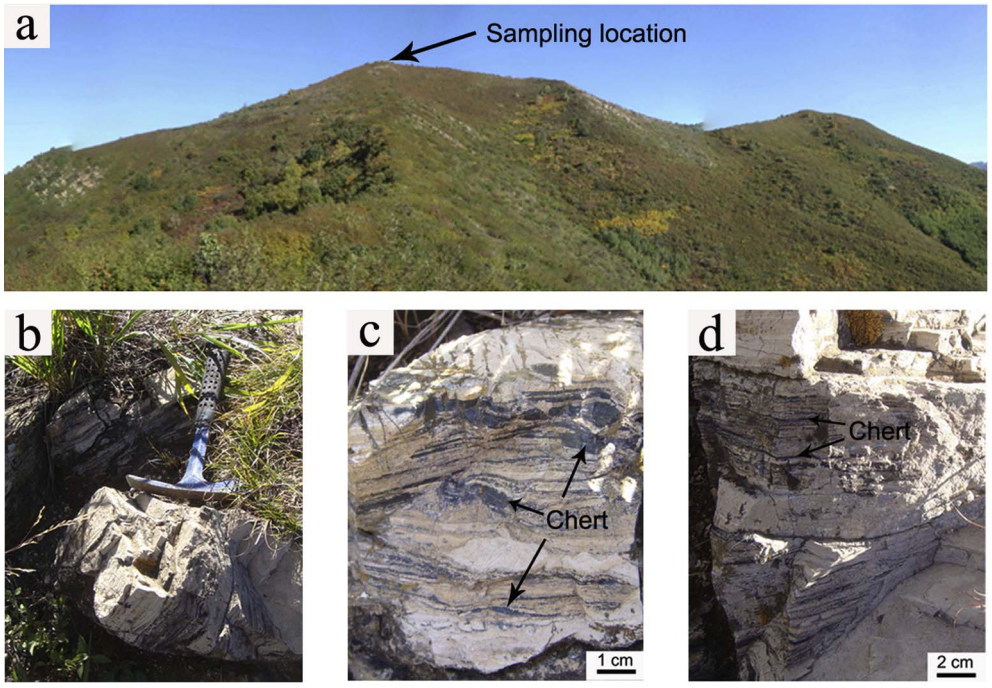

Fig. 1. Sampling location. (a) Overview of the southern mountain of Pangjiapu located in northern China. Arrow indicates the location of the cherty stratiform stromatolites studied. (b) Field photo of cherty stratiform stromatolites. (c, d) Enlarged view of the stromatolites in panel b showing the banded structures. Note that the black bands are organic-rich chert and the white bands are carbonates.

Table 1
Geological background of the study material.

Site	Geologic unit	Age	Lithology	Depositional setting	Fossils
Pangjiapu, China	Gaoyuzhuang Formation	~1500 Ma	Chert and dolomite	Restricted peritidal environment	Cyanobacteria

simultaneously (multi-collection mode) in electron-multipliers (EMs) at a mass resolution of M/△M = 6600. Images obtained from a pre-sputtered area are 256 × 256 pixels and were recorded for ~30 min.

Raman spectra were obtained by use of a LabRAM HR Evolution (Horiba Jobin Yvon) single-stage system having confocal micro-Raman capabilities, following the procedure described in Schopf et al. (2015). Raman images are able to display the spatial distribution of molecular–structural components of both the well-preserved microfossils and their embedding minerals (Schopf et al., 2005, 2015, 2016). Due to the confocal capability of the system, use of a 100× objective provided a horizontal resolution of 1 μm and a vertical resolution of 2 μm. A solid state 532 nm laser was used to obtain the major bands of carbonaceous matter (CM; at ~1350 and ~1605 cm^{-1}) by use of a single spectral window. To avoid spectral artifacts caused by polishing, the laser beam was focused on carbonaceous microfossils beneath the surface of polished thin sections (Ammar and Rouzaud, 2012). 2-D and 3-D Raman imaging was performed using an ultra-fast imaging technique with the acquisition time of 50 ms for each spectrum. The laser power used was ~8 mW over a ~1 μm spot, an instrumental configuration capable of avoiding radiation damage to such specimens (Schopf et al., 2005; Schopf and Kudryavtsev, 2009). To remove the fluorescence background, a linear baseline was subtracted from each spectrum in the range of 900–1900 cm^{-1} (Kouketsu et al., 2014). Peak deconvolution was applied to the identification of complex Raman spectra, following the procedure described in Kouketsu et al. (2014). All 3-D Raman images were processed by use of the CLS fitting method and the 3-D volume rendering method included in Raman software suite LabSpec 6 (Horiba, Edison, NJ).

Confocal fluorescence images were collected with an Olympus Fluoview 1200 CLSM (Olympus, Inc., Shinjuku, Japan) running the FV10-ASW software (v. 3.01) at the University of Cincinnati, following a procedure similar to that described by Czaja et al. (2016). The images shown here were acquired by use of 488 nm laser excitation at 100% transmission (~300 μW at the sample), a 60× oil-immersion objective (NA [numerical aperture] = 1.42) with fluorescence-free microscopy immersion oil (Olympus Type-F), and a 505–605 nm bandpass filter to exclude the incident laser wavelength. All images were subsequently deconvolved to improve X, Y, and Z resolution using Huygens Essentials version 16.10 (Scientific Volume Imaging, The Netherlands) (cf. Schopf and Kudryavtsev, 2009). The 2-D images were exported as TIF files and rendered into 3-D images and animated by use of the software program Paraview v. 5.0.1 (Kitware Inc., Clifton Park, NY).

3. Results

To inform our taphonomic model of cyanobacterial preservation, below we provide morphological information in three dimensions and at submicron spatial resolution, as well as elemental and molecular–structural compositions of rock-embedded microfossils (coccoidal cyanobacteria) from ~1500 Ma Gaoyuzhuang Formation of northern China.

3.1. Electron microscopy

Light microscopy (LM) observations show that abundant coccoidal microfossils are preserved in the organic-rich siliceous layer but not in the carbonate layer of the stromatolites (Fig. 2a–f). SEM observations, combined with LM, aid in distinguishing whether such fossils are exposed at the surface of a thin section or not (Fig. 2g and h). Based on the FIB-milled lamellae, the high-resolution TEM observations (Fig. 3e and f) show that the preserved microfossil wall and sheath are not entirely continuous, which cannot be observed with LM. The bright-field TEM image (Fig. 3e) shows that the curved, semi-continuous microstructure is of lower mass than the surrounding material. Selected area electron diffraction (SAED) carried out in the TEM (Fig. 3g), along with SEM-EDS data in Peng et al. (2016), confirm that the silica infilled the cell interior of the imaged microfossils and can even be found within the fossilized walls and sheaths. These silica grains within carbonaceous structures are sub-spherical, nano-grains, showing an association with CM within the fossilized walls and sheaths (Fig. 3f). These characteristics are an indicator of syngeneity of the fossilized microorganisms with the mineral matrix (Wacey et al., 2012).

3.2. Raman spectroscopy and imagery

The Raman spectra of CM comprising Gaoyuzhuang microfossils were obtained using polished thin sections. The CM Raman spectrum is composed of two intensive bands in the first-order region (1000–1800 cm^{-1}), the G band (~1605 cm^{-1}) and D band (~1350 cm^{-1}), and weaker broad bands in the second-order region (2500–3100 cm^{-1}) (Fig. 4a). The G-band ('G' denotes graphitic; at 1605 cm^{-1}) is assigned to an E_{2g} mode vibration of sp^2-bonded hexagonal ring structures (Ferrari and Robertson, 2000; Qu et al., 2015). The G-band of graphite is commonly located at ~1580 cm^{-1} and can be shifted towards higher wavenumbers due to the confinement effect of the phonons for nanocrystals, such as kerogen and low ordered CM (Ferrari, 2007; Foucher et al., 2015). The D-band is named for a disordered structure and is related to the A_{1g} breathing mode vibration of sp^2 rings in disordered carbonaceous material with defects or heteroatoms in the in-plane domain size of graphene layers (Beyssac et al., 2002; Qu et al., 2015; Dodd et al., 2017).

A compound Raman image of a cluster of coccoidal microfossils (Fig. 4b), acquired in spectral windows centered on the major Raman bands of the materials analyzed (CM at ~1605 cm^{-1} and quartz at ~465 cm^{-1}), shows the relative distribution of CM and the chert matrix (Fig. 4c). The 2-D Raman images of the relative intensity of ~1605 cm^{-1}-band (defined as *I*-1605; Figs. 4d and 6l) indicate the relative abundance of organic carbon of different ultrastructures within individual microfossils. The 2-D Raman image of the relative intensity ratio of ~1350 cm^{-1} versus ~1605 cm^{-1}-band (defined as *I*-1350/1605; Fig. 4e) indicates the structural order of CM comprising microfossils. Using the protocol of Qu et al. (2015), the Raman spectra with intensities of 1350 cm^{-1}- and 1605 cm^{-1}-bands that are lower than c. 5% of the maximum intensities of these two bands in the map were excluded to avoid significant error in the maps of *I*-1350/1605. Previous studies have proposed that a higher *I*-1350/1605 value indicates a higher structural order of CM at peak metamorphic temperature lower than 360 °C (Kouketsu et al., 2014; Sforna et al., 2014; Qu et al., 2015, 2017). Additionally, Raman spectra within the range of 1000–1800 cm^{-1} were deconvoluted into 1172 cm^{-1}-, 1257 cm^{-1}-, 1348 cm^{-1}-, 1490 cm^{-1}-, 1590 cm^{-1}-, 1611 cm^{-1}-, and 1697 cm^{-1}-bands (Fig. 5).

3.3. NanoSIMS analysis

Chemical maps were obtained for most microfossils studied here by use of NanoSIMS. One such example is shown in Fig.6, which shows the elemental distributions of *Eosynechococcus medius* preserved in the

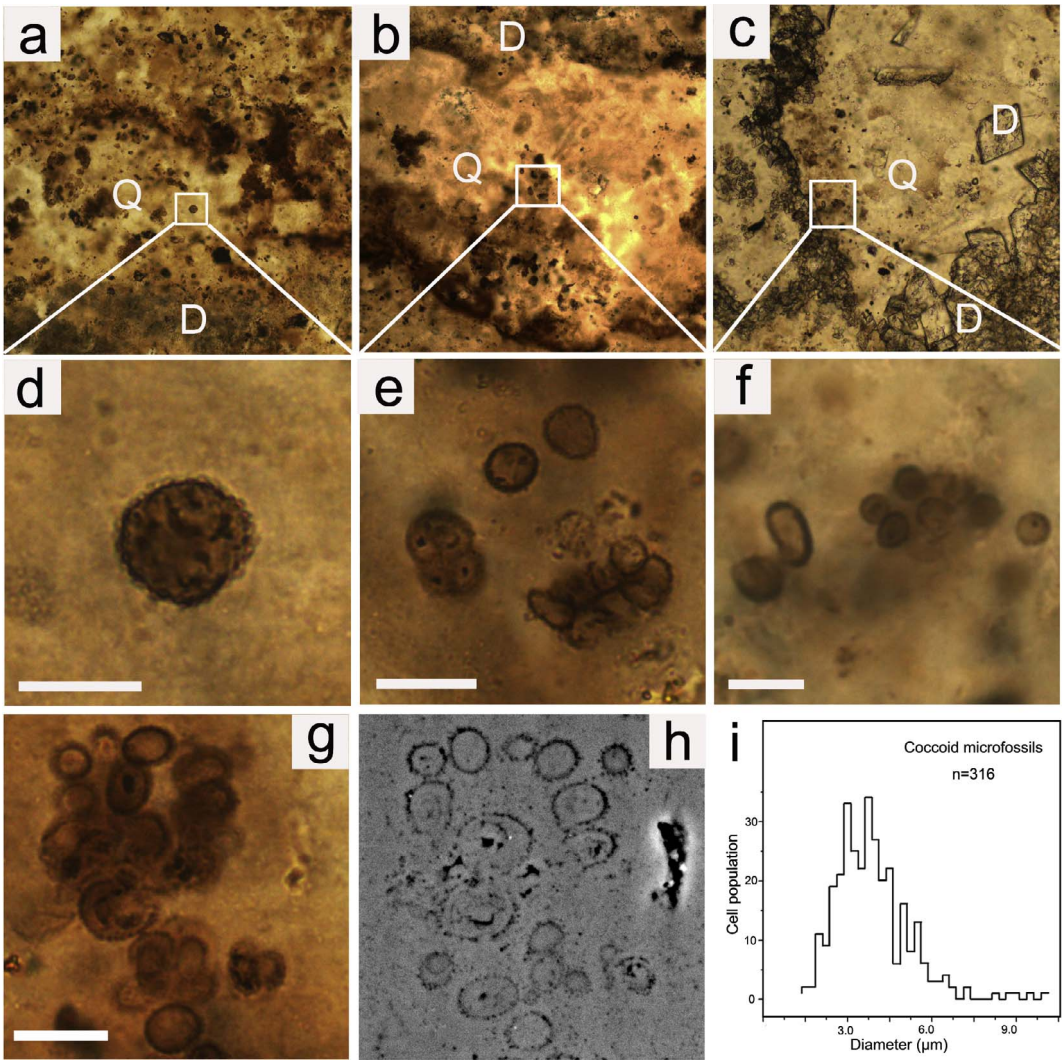

Fig. 2. Light microscopy (LM) and scanning electron microscopy (SEM) photomicrographs of representative cyanobacterial microfossils preserved in the stromatolitic cherts from the ~1500 Ma Gaoyuzhuang Formation. (a, b, d, e) *Glenobotrydion aenigmatis*; among them, panel e shows a tetrad spheroid nucleus mimicking a dividing cell; (c, f) *Eosynechococcus medius*; Note that such cyanobacteria were mainly preserved in the organic-rich siliceous layer of the stromatolites; (g, h) Transmitted-light and SEM images of *Nanococcus vulgaris*, a common species abundant in the Gaoyuzhuang Formation; (i) the cell-size distribution of 316 coccoidal microfossils based on LM photomicrographs. The scale bars are 10 μm for panels d, e and f, but 5 μm for panel g. Q = quartz; D = dolomite.

siliceous layer of a Gaoyuzhuang stromatolite (cf. Fig. 2c and f). The ultra-high-resolution maps show the enrichments of ^{12}C, ^{13}C, $^{12}C^{14}N$, ^{32}S, and ^{34}S, but not of $^{55}Mn^{16}O$ and $^{56}Fe^{16}O_2$ on the microfossil walls (Fig. 6b–h). The ultra-high-resolution maps of ^{13}C versus ^{12}C and ^{34}S versus ^{32}S show the micro-scale isotopic heterogeneities within individual microfossils (Figs. 4f, g and 6j, k). Importantly, these elements are quite consistent with the distribution of organic matter in the cyanobacterial microfossils (Fig. 6). Therefore, the correlated distributions of the metabolically important elements and the microfossils identified by LM, as shown in Fig. 6, provide a biogenic clue for decoding ancient fossil cyanobacteria preserved in the geological record (Oehler et al., 2009; Peng et al., 2016).

3.4. CLSM analysis

Compared with LM and SEM images, 3-D CLSM imaging of the rock-embedded microfossils provides high-resolution morphological information. The laser beam of such systems excites fluorescence emitted from the interlinked polycyclic aromatic hydrocarbons (PAHs) that primarily comprise kerogenous microfossils (Schopf et al., 2005, 2015). As shown in Figs. 7 and 8, CLSM can provide two- and three-dimensional images of coccoidal cyanobacteria at appreciably higher spatial resolution than LM. CLSM images of *Glenobotrydion aenigmatis*, among the most commonly occurring coccoidal cyanobacterial fossils known from the Precambrian, clearly indicate some inclusions within their cell (Fig. 7b and e), potentially providing taxonomically important information. Moreover, the 3-D CLSM images acquired can be rotated to show the cyanobacteria fossils studied from different perspectives (Figs. 7c, f and 8c, f, i; see Supplementary materials for their animations).

4. Discussion

The cell-size distribution of 316 measured individual coccoidal microfossils from the Gaoyuzhuang Formation (Fig. 2i), based on LM images, shows that they range from 1.5 μm to 10.3 μm in diameter, the mean cell diameter is approximately 4 μm, and that the standard deviation (SD) of cell sizes is 1.3 μm (32% of the mean diameter). The distribution is readily distinguishable from coccoidal non-cyanobacterial bacteria and archaea, supporting the classification as chroococcacean cyanobacteria based on morphological observations (Hofmann, 1976; Zhang, 1981; Schopf, 1992, 1996; Seong-Joo et al., 1999; Xu and Awramik, 2002). It is widely acknowledged that the fossilization potential of microbial cells is significantly higher in cherts

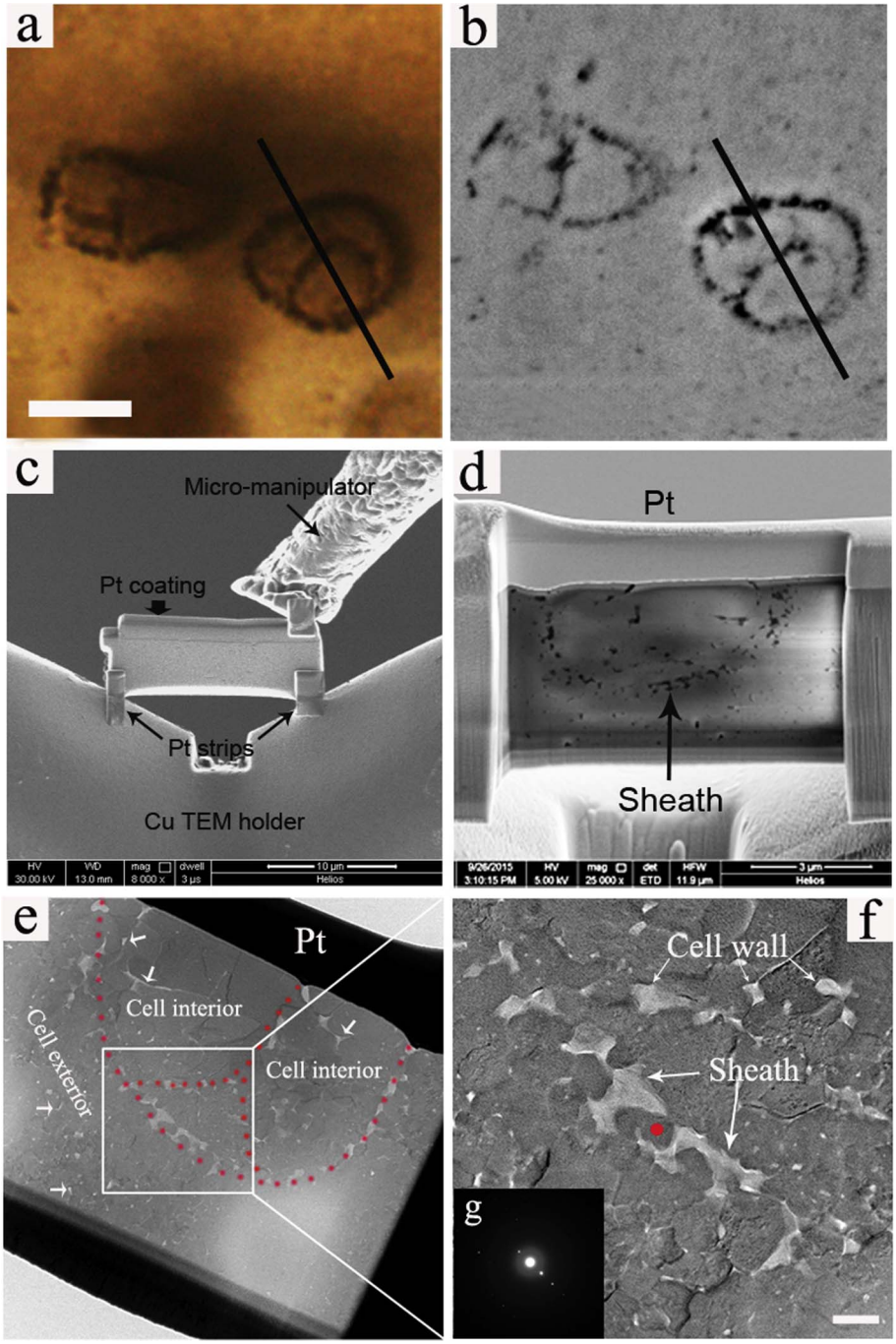

Fig. 3. Correlated light microscopy (LM), scanning electron microscopy (SEM), focused ion beam (FIB) milling – SEM and – TEM photomicrographs of *Eosynechococcus medius* from ~1500 Ma Gaoyuzhuang Formation. (a, b) LM and SEM photomicrographs of such chert-embedded microfossil showing approximate location of FIB milled TEM lamella (black solid lines). (c) Micromanipulation photomicrograph exhibiting the preparation of a FIB-milled ultrathin TEM lamella using the *in situ* lift out technique in a FEI Helios 600i FIB instrument. (d) FIB-SEM photomicrograph showing the microfossil walls and sheaths embedded in chert. (e) Bright-field TEM photomicrograph showing the sketch map of microfossil walls and sheaths (red dash lines). (f) Enlarged view of cell walls and sheaths in panel e, showing a "saw-tooth-like" pattern. (g) SAED pattern showing that the embedded particle (red spot in panel f) within microfossil sheaths are amorphous silica. The scale bar is 5 μm for panel a, but 250 nm for panel f. (For interpretation of the references to colour in this figure legend, the reader is referred to the web version of this article.)

than in other rock types including phosphorites, shales, dolomites, sandstones and limestones (Hofmann, 1976; Kremer et al., 2012; Qu et al., 2017). Even so, the post-mortem silicification of cyanobacterial cells still affects their cellular morphology, chemical composition, and molecular structure to varying degrees (Bartley, 1996; Kremer et al., 2012; Wacey et al., 2012; Alleon et al., 2016). Understanding the taphonomy of cyanobacterial microfossils can help in searching for and identifying the oldest morphological fossils preserved in the geological record.

As mentioned in Section 3.1, the cyanobacterial microfossils from the Gaoyuzhuang Formation were dominantly preserved in stromatolitic cherts (Fig. 2a–f). Previous and current LM observations suggest that Gaoyuzhuang cyanobacterial microfossils can be morphologically classed as "well preserved" (Zhang, 1981; Peng et al., 2016); however, the TEM data indicate that the carbonaceous microfossil walls and sheaths have been impregnated, locally permineralized by silica grains, showing a pattern similar to the "saw-tooth" pattern described by Wacey et al. (2012) (Fig. 3e–g). The sub-spherical nano-silica grains observed in Gaoyuzhuang microfossils are very similar to those precipitated during simulated cyanobacterial silicification in laboratory experiments (Oehler and Schopf, 1971; Benning et al., 2004), as well as natural silicification of hot spring and submarine hydrothermal microbes (Konhauser et al., 2004; Jones et al., 2005, 2008). The association of amorphous silica and CM within fossilized walls and sheaths could potentially be considered as biosignature in the search for traces of past life on the Earth (Wacey et al., 2012; Foucher and Westall, 2013).

Although the angular nano-fragments of carbon scattered along the edges of silica grains in the interior and exterior of microfossils suggest probably diagenetic redistribution of CM during recrystallization of the

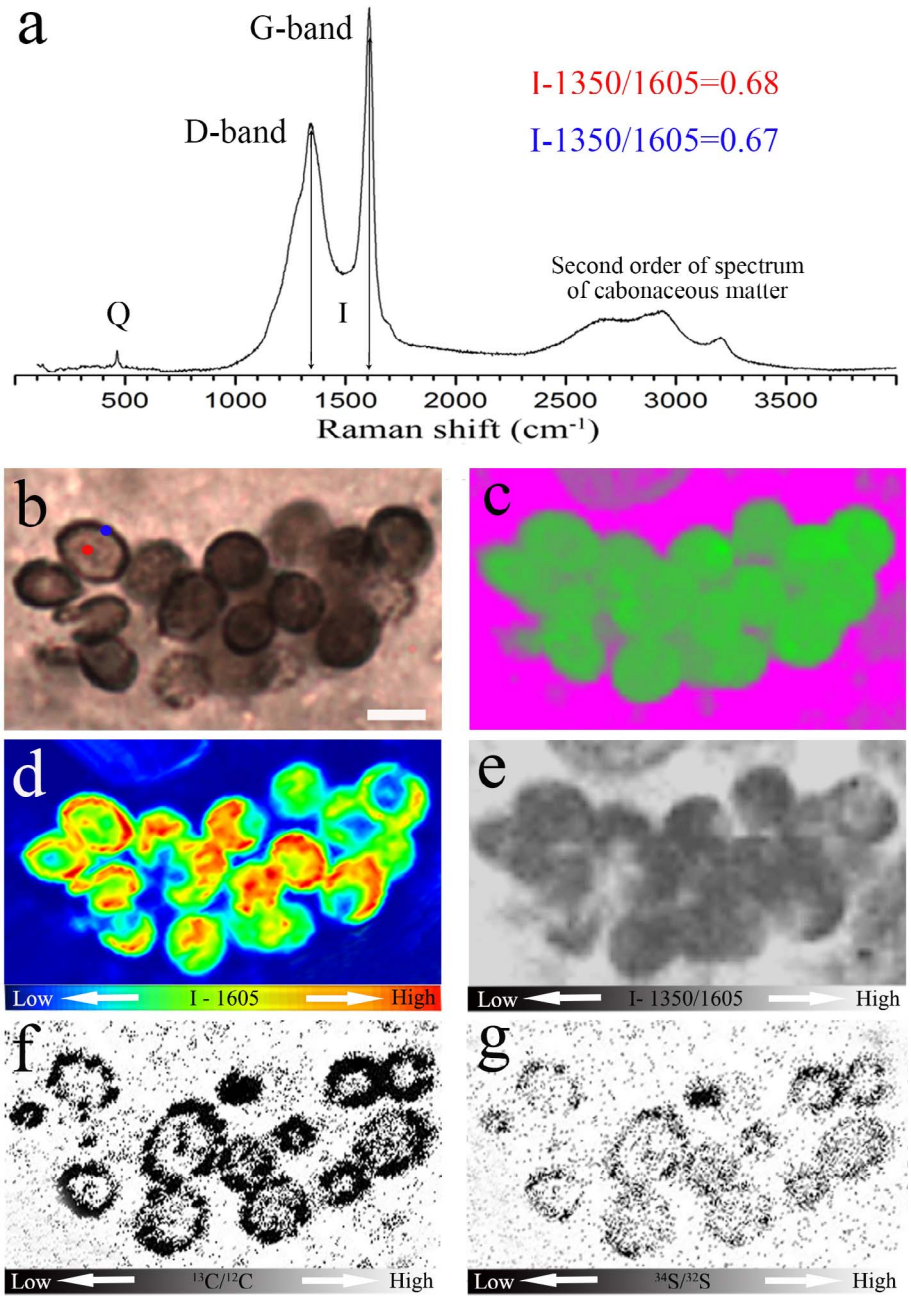

Fig. 4. Raman spectrum and images and their corresponding LM and NanoSIMS images of chert-embedded *Palaeoanacystis vulgaris* from Gaoyuzhuang Formation (~1500 Ma) of northern China. (a) A representative Raman spectrum of a microfossil that shows the two major bands (at ~1350 and ~1605 cm^{-1}) and the second-order band (at 2500–3100 cm^{-1}) of the carbonaceous matter comprising the microfossils as well as of the major band of quartz (at ~465 cm^{-1}); (b) Transmitted-light image of *Palaeoanacystis vulgaris*, the scale bar is 5 μm; the colored spots show the location of the Raman analysis with the calculated parameter *I*-1350/1605 shown on panel a in the corresponding colors; (c) Compound Raman image is acquired in spectral windows centered on the major Raman bands of the materials analyzed: the green image, acquired in a spectral window centered at 1605 cm^{-1}, show the spatial distribution of carbonaceous matter; the pink image, centered at 465 cm^{-1}, show the spatial distribution of quartz (denoted by "Q"); (d) Two-dimensional Raman image of the relative intensity of G-band at 1605 cm^{-1} (defined as *I*-1605), indicating the organic C concentration in the cellular structure; (e) Two-dimensional Raman image of the relative intensity ratio of D-band at 1350 cm^{-1} versus G-band at 1605 cm^{-1} (defined as *I*-1350/1605), showing the cell in the mineral matrix but without obvious subcellular structural variation. (f, g) NanoSIMS maps of the relative concentration ratio of 13C/12C, 34S/32S, respectively, indicating the isotopic heterogeneities in the cytoarchitectures. (For interpretation of the references to colour in this figure legend, the reader is referred to the web version of this article.)

matrix silica (e.g., arrowed in Fig. 3e), almost intact microfossil colonies can be visually observed by their 3-D CLSM images and animations (Figs. 7c, f and 8c, f, i; see Supplementary materials for their animations). The rough microfossil walls and sheaths, consistent with a saw-tooth-like pattern in the distribution of microfossil carbon (cf. Fig. 3f), is likely to result from degradation prior to or/and during silicification; however the coccoidal morphology is still clearly visible (Figs. 7 and 8). Such preservation in three dimensions likely suggests that cyanobacteria were silicified very rapidly after death, even when still alive, indicating the very early diagenetic emplacement of silica prior to degradational collapse (Butterfield, 2003; Wacey et al., 2012). Some apparent internal complexities are shown within spheroidal *Glenobotrydion* microfossils (Fig. 7b and c), probably representing degraded cell contents (Knoll and Golubic, 1979; Zhang, 1981). The three-dimensional morphologies of other cyanobacterial taxa (*Eosynechococcus*, *Nanococcus*, and *Palaeoanacystis*) show apparent different internal structures (Fig. 8), potentially aiding in fossil taxonomy.

To further assess the molecular preservation of Gaoyuzhuang organic microfossils, Raman spectra were deconvolved into seven subsidiary bands (Fig. 5). Two sub-bands (at 1172 and 1257 cm^{-1}, respectively) can be identified as broad shoulders on the low-frequency side of the D band at 1348 cm^{-1} (Fig. 5). The band at 1172 cm^{-1} is very weak in the spectra measured here, but is widely interpreted as the symmetric stretch of C—C single bonds of C—C=C—C bridges between aromatic domains (Schafer et al., 1991; Schopf et al., 2005; Ferralis et al., 2016). The band at 1257 cm^{-1} is assigned to the vibrations of methyl groups in alkane chains or/and deformation modes in fatty acids (Koyama and i Ikeda, 1980). These peaks can often be detected in fairly immature CM or functionalized carbon systems including fatty acids but not in highly carbonized or purely graphitic materials (Koyama and i Ikeda, 1980; De Gelder et al., 2007). Therefore, the appearance of such peaks is an indicator for well-preserved (less geochemically altered) molecular signatures of rock-embedded organic microfossils (Schopf et al., 2005; Ferralis et al., 2016; Alleon et al., 2016). The other non-

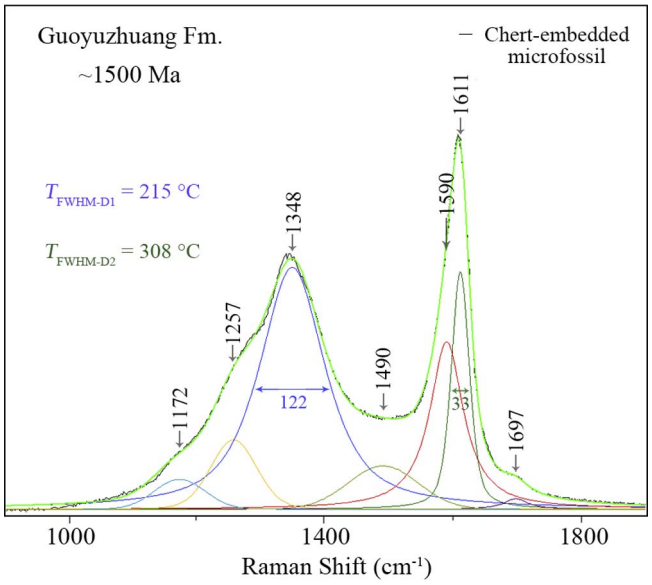

Fig. 5. Representative Raman spectrum of a chert-embedded *Palaeoanacystis vulgaris* from Gaoyuzhuang Formation (~1500 Ma) of northern China (Figs. 4b and 8g) and results of deconvolution of the spectrum acquired *in situ* showing it to be composed of seven subsidiary bands. The peak metamorphic temperature is estimated by using the equations described in Kouketsu et al. (2014). The full width half maximum (FWHM) values of the D1 and D2 bands are 122 and 33 cm^{-1}, respectively. Note that the temperature estimation using FWHM-D1 is commonly more reliable than that using FWHM-D2.

aromatic sub-band (at 1697 cm^{-1}; Fig. 5) is interpreted as the symmetric stretch vibration of C═O carbonyl groups in aliphatic esters, aldehydes and ethers, probably representing the bridging links between kerogenous aromatic domains (Siskin and Katritzky, 1991). Given its heat-labile nature, the occurrence of such a band has the potential to indicate that Gaoyuzhuang cyanobacterial microfossils have not experienced a high diagenetic temperature (Schopf et al., 2005). This is consistent with an estimation of a low-grade metamorphic temperature of 215–308 °C using the full width half maximum values of the D1 and D2 bands (122 and 33 cm^{-1}, respectively; Fig. 5) and the equations described in Kouketsu et al. (2014).

The peak metamorphic temperature cannot explain the micro-scale structural heterogeneities observed in our fossils (Figs. 4 and 6; Kouketsu et al., 2014), and we can rule out any factors that could have masked the molecular structure of CM in the fossils. Thin-section polishing artifacts can be excluded because Raman spectra were acquired beneath the polished surface (Ammar and Rouzaud, 2012). The mineral-templating effect described by van Zuilen et al. (2012) has also been not observed in Gaoyuzhuang microfossils (Fig. 3f), potentially implying that this process might occur during pre-graphitization/graphitization at temperature above 300 °C (van Zuilen et al., 2012; Foucher et al., 2015). Given no evidence of shear deformation and hydrothermal fluid deposition of graphite (Aoya et al., 2010; Lepland et al., 2011), the nature of CM preserved in Gaoyuzhuang cyanobacterial microfossils can reveal the structural and chemical properties of the carbonaceous precursor (Sforna et al., 2014; Foucher et al., 2015; Qu et al., 2015, 2017).

Raman maps of Gaoyuzhuang cyanobacterial microfossils show no obvious cellular-scale molecular-structural variation within individual microfossils (Fig. 4e). As Qu et al. (2015) noted, this might be caused by the simple cell structure and a lack of organelles, potentially providing additional evidence for distinguishing prokaryotic cyanobacteria from eukaryotic cells preserved in the geological record. The heterogeneous NanoSIMS maps of ^{13}C versus ^{12}C and ^{34}S versus ^{32}S for cyanobacterial microfossils studied here (Figs. 4f, g and 6j, k), although unstandardized, probably reveal differences in the original isotopic composition of different cytoarchitectures, such as sub-cellular components (Qu et al., 2017). These cyanobacteria inside the polished thin section have unbroken globular microfossil walls (Figs. 7c, f and 8c, f, i; see Supplementary materials for their animations), further supporting the subcellular isotopic and chemical heterogeneities recorded in NanoSIMS maps. The micro-scale chemical (Fig. 6b–f and i), isotopic (Figs. 4f, g and 6j, k) and structural (Figs. 3e, f, 4d, e and 6l) heterogeneities together with the subcellular morphological features (Figs. 7 and 8) strongly indicate that the cyanobacterial cell walls have been preserved nearly intact by silicification although most cell contents were degraded (Knoll and Golubic, 1979; Zhang, 1981; Schultze-Lam et al., 1995; Bartley, 1996; Peng et al., 2016).

The absence of systematic variations in micro-scale molecular-structural order (Fig. 4) suggests a similar composition for all cyanobacterial cell walls analyzed, consistent with the identical elemental distributions recorded in NanoSIMS maps (Fig. 6). These maps also indicate nearly identical elemental distributions to those reported by Peng et al. (2016) despite the fact that study analyzed different cyanobacterial taxa. One explanation for this phenomenon is that the extracellular polymeric substances of cyanobacteria may be capable of forming organic chelate compounds by binding the heavy metals such as iron to resist post-mortem degradation (Golubic and Barghoorn, 1977; Ferris et al., 1988). Another possibility is that cyanobacterial sheaths are composed principally of cross-linked polysaccharides containing phenolic elements, which potentially accounts for its durability in preservation (Krumbein and Swart, 1983; Robbins, 1992; Bartley, 1996). The latter may be the most plausible explanation because of no metal enrichment on microfossil walls detected using NanoSIMS (see Section 3.3). Post depositional diagenetic alteration also likely played a role in removing minor labile molecular-structural components of the cell walls to increase the similarity of the preserved CM.

Our data about morphological, chemical and molecular structural preservation of the 1500 Ma Gaoyuzhuang microfossils can be used as a baseline to assess other cyanobacterial and other microbial microfossils permineralized in Archean cherts. Based on their restricted peritidal environment (Table 1; Seong-Joo and Golubic, 1999; Xu and Awramik, 2002), we propose a probable taphonomic model for Gaoyuzhuang cyanobacteria, potentially responsible for the fidelity of preservation. In the first stage, abundant silica derived from continental weathering and/or from a hydrothermal vent is dissolved in seawater inhabited by cyanobacteria, possibly resulting in the local formation of silica colloid (Oehler and Schopf, 1971). Cyanobacteria would have been entirely impregnated by a solution of colloidal silica, prior to their degradation (Butterfield, 2003). The highly cross-linked nature of cyanobacterial cell walls and sheaths ensures the preferential preservation of these structures over cell contents (Robbins, 1992; Bartley, 1996). In the second stage, the colloidal silica is transformed in steps into a gel state by evaporation of seawater in the restricted environment (Iller, 1979; Benning et al., 2005). Under a temperature not more than 215–308 °C, the relatively rapid crystallization of chert from silica gel would have been responsible for the intact preservation of ancient cyanobacteria (Ferris et al., 1988; Bartley, 1996; Jones et al., 2004; Kremer et al., 2012; Peng et al., 2013). In the last stage, sea level fluctuation would have resulted in the alternate precipitation of silica and carbonate, ultimately leading to the formation of fossiliferous stromatolitic cherts favorable for the resistance to post-mortem diagenetic alteration. The taphonomic model proposed here has potential for providing crucial information about the formation and preservational conditions of cyanobacterial microfossils preserved in cherts from throughout the Precambrian.

5. Conclusions and implications

The Gaoyuzhuang microfossil assemblage (~1500 Ma; Peng et al., 2016), which includes some of the best-preserved ancient cyanobacteria, has attracted increasing interest in terms of exploring early life on Earth, but its cellular taphonomy has not been widely reported until

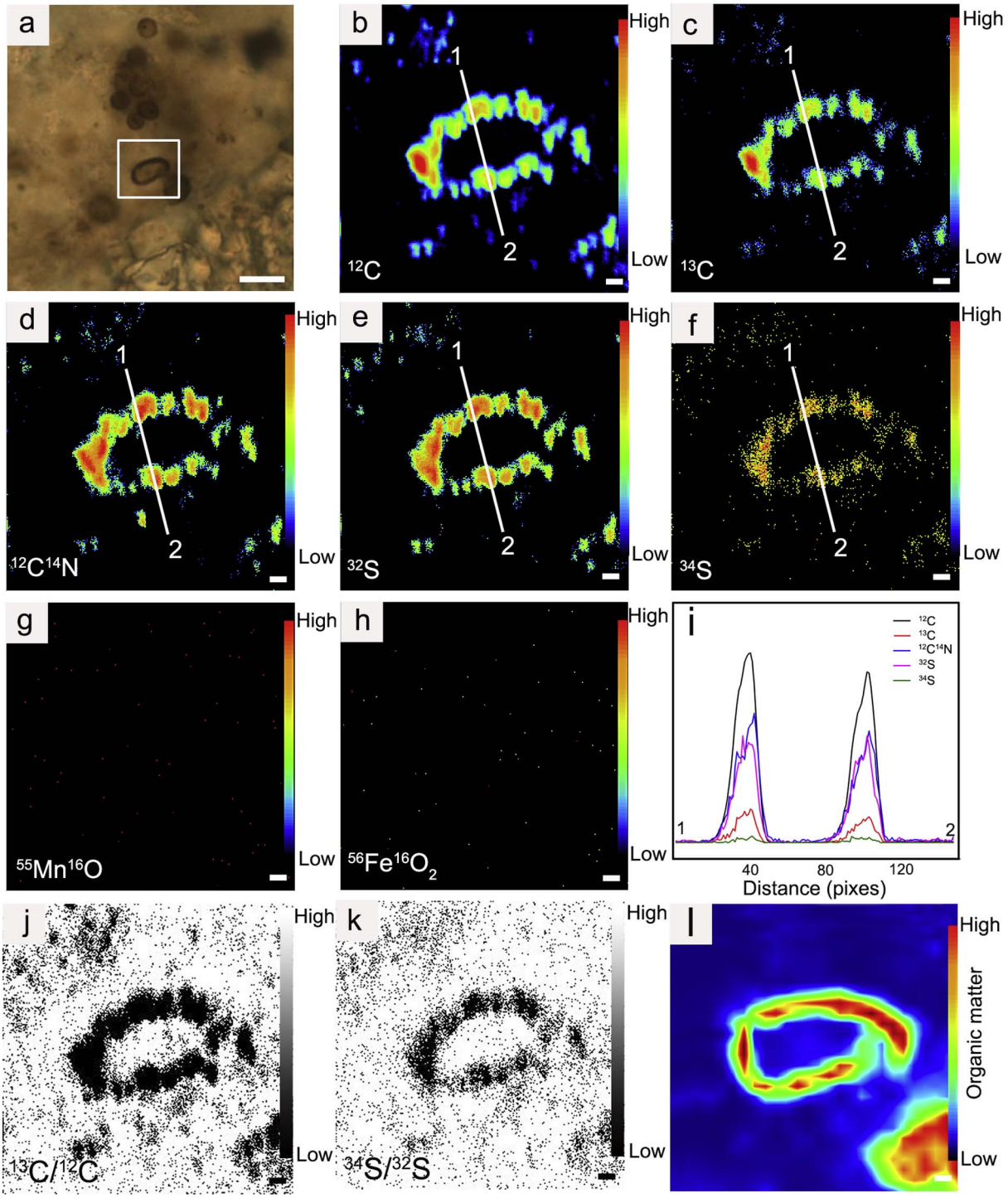

Fig. 6. Correlated LM, NanoSIMS and Raman images of a representative cyanobacterium (*Eosynechococcus medius*) preserved in the stromatolitic cherts from the ~1500 Ma Gaoyuzhuang Formation. (a) Transmitted light photograph (same fossils illustrated in Fig. 2f); (b–h) Ion images of ^{12}C, ^{13}C, $^{12}C^{14}N$, ^{32}S, ^{34}S, $^{55}Mn^{16}O$, and $^{56}Fe^{16}O_2$, respectively; (i) Profiles along white solid line (1–2) in panels b–f; (j, k) NanoSIMS maps of the relative concentration ratio of $^{13}C/^{12}C$, $^{34}S/^{32}S$, respectively, indicating the isotopic heterogeneities in the cytoarchitectures. (l) Two-dimensional Raman image of *I*-1605, showing the spatial distribution of organic matter on the surface of polished thin section. Ion intensity variations are shown by the calibration bar. The scale bar is 10 μm for panel a, but 1 μm for panels b–h and j–l.

now. In this study, combined *in situ* microscopic and microanalytical techniques were employed to provide Raman, NanoSIMS and CLSM images on Mesoproterozoic cyanobacterial fossils, potentially identifying the molecular structural, chemical, isotopic characteristics and organismal morphology of rock-embedded microfossils in three dimensions and at submicron spatial resolution. Further, we proposed a probable taphonomic model responsible for the fidelity of preservation for Gaoyuzhuang cyanobacteria. Given the prevalent existence of such environments on the early Earth, this taphonomic model proposed here may have occurred in other strata, such as the well-known Gunflint Formation of Ontario, Canada (~1880 Ma; Barghoorn and Tyler, 1965), Avzyan Formation of Russian Federation (~1200 Ma; Sergeev, 1994) and Bitter Springs Formation of central Australia (~830 Ma; Schopf, 1968). Therefore, our data are capable of providing significant insight into the preservation of ancient cyanobacteria and other types of microorganisms in Archean rocks.

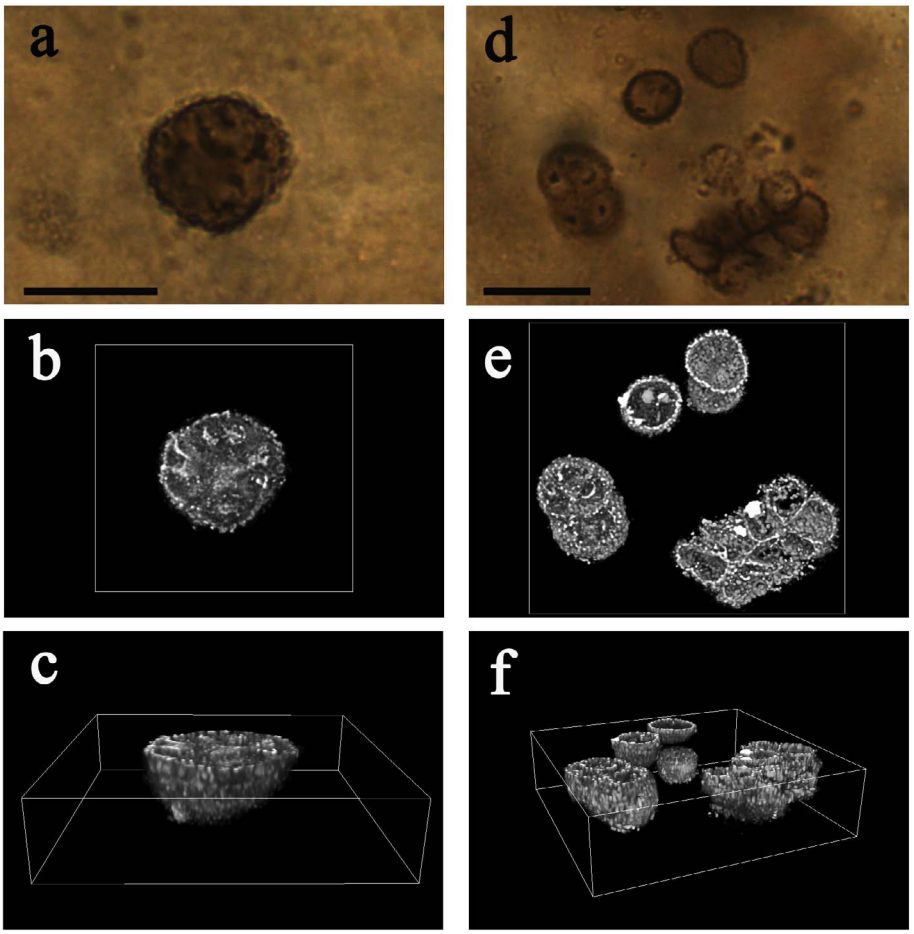

Fig. 7. Correlated LM and CLSM photomicrographs of chert-permineralized *Glenobotrydion aenigmatis* from Gaoyuzhuang Formation (the southern mountain of Pangjiapu, Hebei Province, China). (a, d) Transmitted light images (same fossils illustrated in Fig. 2d and e, respectively); (b, c, e, and f) Three-dimensional CLSM images viewed in the plane of the thin section (b and e) and rotated to an oblique view (c and f); Note apparent internal complexity within such microfossils potentially representing degraded cell contents. All scale bars in LM images are 10 μm.

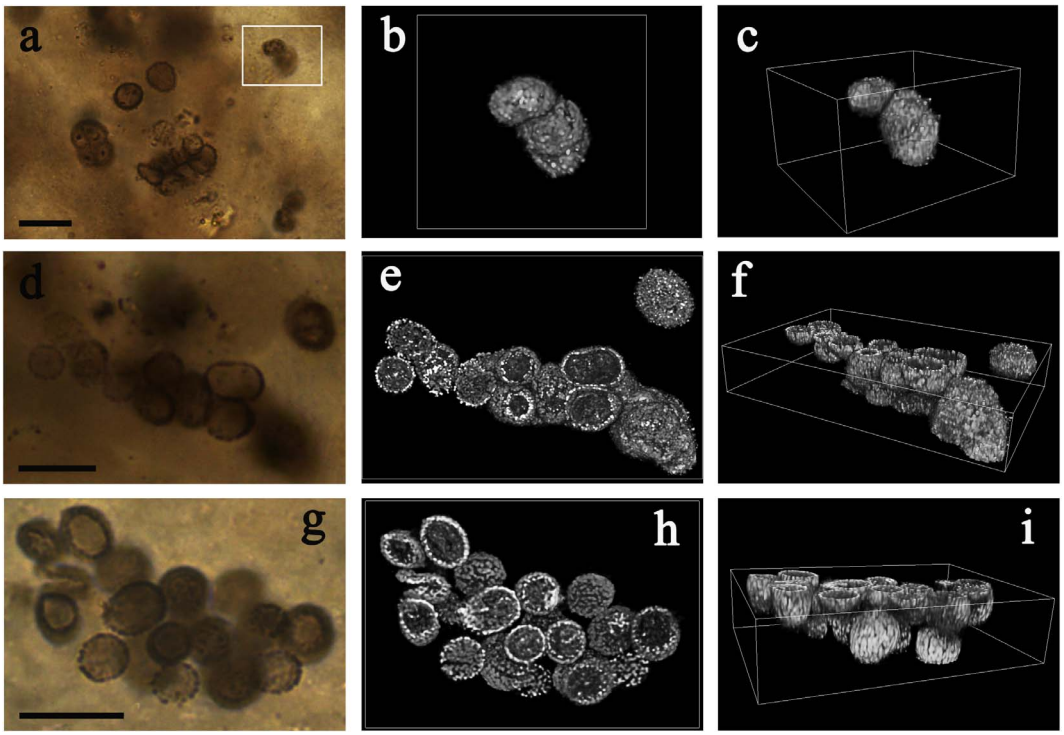

Fig. 8. Comparison of chert-permineralized cyanobacterial microfossils from Gaoyuzhuang Formation (the southern mountain of Pangjiapu, Hebei Province, China) with microfossils analyzed *in situ*, in petrographic thin sections, imaged by LM (a, d, g), and three-dimensional CLSM in the plane of the thin section (b, e, h) and rotated to an oblique view (c, f, i). (a–c) *Eosynechococcus medius*; (d–f) *Nanococcus vulgaris*; (g–i) *Palaeoanacystis vulgaris* (same fossils shown in Fig. 4). All scale bars in LM images are 10 μm.

Acknowledgments

This work was directly supported by the Strategic Priority Research Program of the Chinese Academy of Sciences (XDB06020000) and the National Key Basic Research Program of China (2015CB755905). We are indebted to Jialong Hao, Jianchao Zhang for analytical assistance at the Institute of Geology and Geophysics, Chinese Academy of Sciences, Enping Hu for analytical assistance at the Horiba (China) Trading Co., Ltd, and Xue Liang for analytical assistance at Shanghai University. This manuscript was improved by thoughtful comments from Y. Qu and three anonymous reviewers.

Appendix A. Supplementary data

Supplementary data associated with this article can be found, in the online version, at http://dx.doi.org/10.1016/j.precamres.2017.11.007.

References

Alleon, J., Bernard, S., Le Guillou, C., Marin-Carbonne, J., Pont, S., Beyssac, O., McKeegan, K.D., Robert, F., 2016. Molecular preservation of 1.88 Ga Gunflint organic microfossils as a function of temperature and mineralogy. Nat. Commun. 7, 11977. http://dx.doi.org/10.1038/ncomms11977.

Altermann, W., Schopf, J.W., 1995. Microfossils from the Neoarchean Campbell Group, Griqualand West Sequence of the Transvaal Supergroup, and their paleoenvironmental and evolutionary implications. Precambr. Res. 75, 65–90.

Ammar, M.R., Rouzaud, J.N., 2012. How to obtain a reliable structural characterization of polished graphitized carbons by Raman microspectroscopy. J. Raman Spectrosc. 43, 207–211.

Aoya, M., Kouketsu, Y., Endo, S., Shimizu, H., Mizukami, T., Nakamura, D., Wallis, S., 2010. Extending the applicability of the Raman carbonaceous-material geothermometer using data from contact metamorphic rocks. J. Metamorph. Geol. 28, 895–914.

Barghoorn, E.S., Tyler, S.A., 1965. Microorganisms from Gunflint Chert. Science 147, 563–577.

Bartley, J., 1996. Actualistic Taphonomy of Cyanobacteria: Implications for the Precambrian Fossil Record. Palaios 11, 571–586.

Benning, L.G., Phoenix, V.R., Yee, N., Konhauser, K.O., 2004. The dynamics of cyanobacterial silicification: an infrared micro-spectroscopic investigation. Geochim. Cosmochim. Acta 68, 743–757.

Benning, L.G., Phoenix, V., Mountain, B.W., 2005. Biosilicification: the role of cyanobacteria in silica sinter deposition. In: Gadd, G.M., Semple, K.T., Lapin-Scott, H.M. (Eds.), Micro-Organisms and Earth Systems-Advances in Geomicrobiology, SGM Symposium 65. Cambridge University Press, Cambridge, pp. 131–150.

Beyssac, O., Goffe, B., Chopin, C., Rouzaud, J.N., 2002. Raman spectra of carbonaceous material in metasediments: a new geothermometer. J. Metamorphic Geol. 20, 859–871.

Butterfield, N.J., 2003. Exceptional fossil preservation and the Cambrian explosion. Integr. Comp. Biol. 43, 166–177.

Czaja, A.D., Beukes, N.J., Osterhout, J.T., 2016. Sulfur-oxidizing bacteria prior to the Great Oxidation Event from the 2.52 Ga Gamohaan Formation of South Africa. Geology 44 (12), 983–986.

De Gelder, J., De Gussem, K., Vandenabeele, P., Moens, L., 2007. Reference database of Raman spectra of biological molecules. J. Raman Spectrosc. 38 (9), 1133–1147.

Dodd, M.S., Papineau, D., Grenne, T., Slack, J.F., Rittner, M., Pirajno, F., O'Neil, J., Little, C.T.S., 2017. Evidence for early life in Earth's oldest hydrothermal vent precipitates. Nature 543, 60–65.

Ferralis, N., Matys, E.D., Knoll, A.H., Hallmann, C., Summons, R.E., 2016. Rapid, direct and non-destructive assessment of fossil organic matter via microRaman spectroscopy. Carbon 108, 440–449.

Ferrari, A.C., 2007. Raman spectroscopy of graphene and graphite: disorder, electron–phonon coupling, doping and nonadiabatic effects. Solid State Commun. 143, 47–57.

Ferrari, A.C., Robertson, J., 2000. Interpretation of Raman spectra of disordered and amorphous carbon. Phys. Rev. B 61, 14095–14107.

Ferris, F.G., Fyfe, W.S., Beveridge, T.J., 1988. Metallic ion binding by *Bacillus subtilis*: implications for the fossilization of microorganisms. Geology 16, 149–152.

Foucher, F., Westall, F., 2013. Raman imaging of metastable opal in carbonaceous microfossils of the 700–800Ma Old Draken Formation. Astrobiology 13, 57–67.

Foucher, F., Ammar, M.R., Westall, F., 2015. Revealing the biotic origin of silicified Precambrian carbonaceous microstructures using Raman spectroscopic mapping, a potential method for the detection of microfossils on Mars. J. Raman Spectrosc. 46, 873–879.

Golubic, S., Barghoorn, E.S., 1977. Interpretation of microbial fossils with special reference to the Precambrian. In: Flugel, E. (Ed.), Fossil Algae. Springer, Berlin, pp. 1–14.

Golubic, S., Seong-Joo, L., 1999. Early cyanobacterial fossil record: preservation, palaeoenvironments and identification. Eur. J. Phycol. 34 (4), 339–348. http://dx.doi.org/10.1080/09670269910001736402.

Hofmann, H.J., 1976. Precambrian microflora, Belcher Islands, Canada: significance and systematics. J. Paleontol. 50, 1040–1073.

House, C.H., Schopf, J.W., McKeegan, K.D., Coath, C.D., Harrison, T.M., Stetter, K.O., 2000. Carbon isotopic composition of individual Precambrian microfossils. Geology 28, 707–710.

Iller, R.K., 1979. The Chemistry of Silica: Solubility, Polymerization, Colloid and Surface Properties, and Biochemistry. John Wiley & Sons, New York.

Jones, B., Konhauser, K.O., Renaut, R.W., Wheeler, R.S., 2004. Microbial silicification in Iodine Pool, Waimangu geothermal area, North Island, New Zealand: implications for recognition and identification of ancient silicified microbes. J. Geol. Soc. London 161, 983–993.

Jones, B., Renaut, R.W., Konhauser, K.O., 2005. Genesis of large siliceous stromatolites at Frying Pan Lake, Waimangu geothermal field, North Island, New Zealand. Sedimentology 52, 1229–1252.

Jones, B., de Ronde, C.E.J., Renaut, R.W., 2008. Mineralized microbes from Giggenbach submarine volcano. J. Geophys. Res. 113, B08S05.

Knoll, A.H., Golubic, S., 1979. Anatomy and taphonomy of a Precambrian algal stromatolite. Precambr. Res. 10, 115–151.

Konhauser, K.O., Jones, B., Phoenix, V.R., Ferris, F.G., Renaut, R.W., 2004. The microbial role in hot spring silicification. Ambio 33, 552–558.

Kouketsu, Y., Mizukami, T., Mori, H., Endo, S., Aoya, M., Hara, H., Nakamura, D., Wallis, S., 2014. A new approach to develop the Raman carbonaceous material geothermometer for low-grade metamorphism using peak width. Island Arc 23, 33–50.

Koyama, Y., i Ikeda, K., 1980. Raman spectra and conformations of the cis-unsaturated fatty-acid chains. Chem. Phys. Lipids 26 (2), 149–172.

Kremer, B., Kazmierczak, J., Łukomska-Kowalczyk, M., Kempe, S., 2012. Calcification and silicification: fossilization potential of Cyanobacteria from Stromatolites of Niuafo'ou's Caldera Lakes (Tonga) and implications for the early fossil record. Astrobiology 12, 535–548.

Krumbein, W.E., Swart, P.K., 1983. The microbial carbon cycle. In: Krumbein, W.E. (Ed.), Microbial Geochemistry Blackwell. Oxford, pp. 5–62.

Lepland, A., van Zuilen, M.A., Philippot, P., 2011. Fluid deposited graphite and its geobiological implications in early Archean gneiss from Akilia, Greenland. Geobiology 9, 2–9.

Licari, G.R., Cloud Jr., P.E., Smith, W.D., 1969. A new chroococcacean alga from the Proterozoic of Queensland. Proc. Nat. Acad. Sci. U.S.A. 62, 56–62.

Oehler, J.H., Schopf, J.W., 1971. Artificial microfossils: experimental studies of permineralization of blue-green algae in silica. Science 174, 1229–1231.

Oehler, D.Z., Robert, F., Walter, M.R., Sugitani, K., Allwood, A., Meibom, A., Mostefaoui, S., Selo, M., Thomen, A., Gibson, E.K., 2009. NanoSIMS: insights to biogenicity and syngeneity of Archaean carbonaceous structures. Precambr. Res. 173, 70–78.

Ogurtsova, R.N., Sergeev, V.N., 1987. Mikrobiota chichkanskoj svity verkhnego dokembriya Malago Karatau (Yuzhnyj Kazakhstan) [Microbiota of the Chichkan Formation, Little Karatau Range (South Kazakhstan)]. Paleontal. Zhur. 2, 107–116 (in Russian).

Peng, X., Xu, H., Jones, B., Chen, S., Zhou, H., 2013. Silicified virus-like nanoparticles in an extreme thermal environment: implications for the preservation of viruses in the geological record. Geobiology 11, 511–526.

Peng, X., Guo, Z., House, C.H., Chen, S., Ta, K., 2016. SIMS and NanoSIMS analyses of well-preserved microfossils imply oxygen-producing photosynthesis in the Mesoproterozoic anoxic ocean. Chem. Geol. 441, 24–34.

Qu, Y., Engdah, A., Zhu, S., Vajda, V., McLoughlin, N., 2015. Ultrastructural heterogeneity of carbonaceous material in ancient cherts: investigating biosignature origin and preservation. Astrobiology 825–842.

Qu, Y., Wang, J., Xiao, S., Whitehouse, M., Engdahl, A., Wang, G., McLoughlin, N., 2017. Carbonaceous biosignatures of diverse chemotrophic microbial communities from chert nodules of the Ediacaran Doushantuo Formation. Precambr. Res. 290, 184–196.

Robbins, R., 1992. Biochemistry of the Sheath of the Cyanobacterium Lyngbya aestuarii. Unpublished Ph.D. Dissertation. University of California, Los Angeles, California, pp. 169.

Schafer, H.E., Chance, R.R., Sibley, R.J., Knoll, K., Schrock, R.R., 1991. Conjugation length dependence of Raman scattering in a series of linear polyenes: implications for polyacetylene. J. Chem. Phys. 94, 4161–4170.

Schopf, J.W., 1968. Microflora of the Bitter Springs formation, late Precambrian, Central Australia. J. Paleontol. 42, 651–688.

Schopf, J.W., 1992. Proterozoic prokaryotes: affinities, geologic distribution and evolutionary trends. In: Schopf, J.W., Klein, C. (Eds.), The Proterozoic Biosphere: A Multidisciplinary Study. Cambridge University Press, Cambridge, UK, pp. 195–218.

Schopf, J.W., 1993. Microfossils of the early Archean Apex chert: new evidence of the antiquity of life. Science 260, 640–646.

Schopf, J.W., 1996. Cyanobacteria: pioneers of the early Earth. Nova Hedwigia 112, 13–32.

Schopf, J.W., 2002. The fossil record: tracing the roots of the cyanobacterial lineage. In: Whitton, B.A., Potts, M. (Eds.), The Ecology of Cyanobacteria, pp. 13–35.

Schopf, J.W., Kudryavtsev, A.B., 2009. Confocal laser scanning microscopy and Raman imagery of ancient microscopic fossils. Precambr. Res. 173, 39–49.

Schopf, J.W., Kudryavtsev, A.B., 2012. Biogenicity of Earth's earliest fossils: a resolution of the controversy. Gondwana Res. 39, 761–771.

Schopf, J.W., Packer, B.M., 1987. Early Archean (3.3-billion to 3.5-billion-year-old) microfossils from Warrawoona Group, Australia. Science 237, 70–73.

Schopf, J.W., Ford, T.D., Breed, W.J., 1973. Microorganisms from the late Precambrian of the Grand Canyon, Arizona. Science 179, 1319–1321.

Schopf, J.W., Zhu, W.-Q., Zu, Z.L., Hsu, J., 1984. Proterozoic stromatolitic microbiotas of the 1400–1500 Ma-old Gaoyuzhuang Formation near Jixian, Northern China. Precambr. Res. 24, 335–349.

Schopf, J.W., Kudryavtsev, A.B., Agresti, D.G., Czaja, A.D., Wdowiak, T.J., 2005. Raman imagery: a new approach to assess the geochemical maturity and biogenicity of permineralized Precambrian fossils. Astrobiology 5, 333–371.

Schopf, J.W., Sergeev, V.N., Kudryavtsev, A.B., 2015. A new approach to ancient microorganisms: taxonomy, paleoecology, and biostratigraphy of the Lower Cambrian Berkuta and Chulaktau microbiotas of South Kazakhstan. J. Paleontol. 89, 695–729. http://dx.doi.org/10.1017/jpa.2015.56.

Schopf, J.W., Calça, C.P., Garcia, A.K., Kudryavtsev, A.B., Souza, P.A., Félix, C.M., Fairchild, T.R., 2016. In situ confocal laser scanning microscopy and Raman spectroscopy of bisaccate pollen from the Irati Subgroup (Permian, Paraná Basin, Brazil): comparison with acid-macerated specimens. Rev. Palaeobot. Palynol. 233, 169–175.

Schultze-Lam, S., Ferris, F.G., Konhauser, K.O., Wiese, R.G., 1995. In situ silicification of an Icelandic hot spring microbial mat: implications for microfossil formation. Can. J. Earth Sci. 32, 2021–2026.

Seong-Joo, L., Golubic, S., 1999. Microfossil populations in the context of synsedimentary micrite deposition and acicular carbonate precipitation: mesoproterozoic Gaoyuzhuang Formation, China. Precambr. Res. 96, 183–208.

Seong-Joo, L., Golubic, S., Verrecchia, E., 1999. Epibiotic relationships in Mesoproterozoic fossil record: Gaoyuzhuang Formation, China. Geology 27, 1059–1062.

Sergeev, V.N., 1994. Microfossils in cherts from the Middle Riphean (Mesoproterozoic) Avzyan Formation, southern Ural Mountains, Russian Federation. Precambr. Res. 65, 231–254.

Sergeev, V.N., Schopf, J.W., 2010. Taxonomy, paleoecology and biostratigraphy of the Late Neoproterozoic Chichkan microbiota of south Kazakhstan: the marine biosphere on the eve of metazoan radiation. J. Paleontol. 84, 363–401.

Sforna, M., van Zuilen, M., Philippot, P., 2014. Structural characterization by Raman hyperspectral mapping of organic carbon in the 3.46 billion-year-old Apex chert, Western Australia. Geochim. Cosmochim. Acta 124, 18–33.

Shih, P.M., Hemp, J., Ward, L.M., Matzke, N.J., Fischer, W.W., 2017. Crown group Oxyphotobacteria postdate the rise of oxygen. Geobiology 15, 19–29.

Siskin, M., Katritzky, A.R., 1991. Reactivity of organic compounds in hot water: geochemical and technological implications. Science 254, 231–237.

Soo, R.M., Hemp, J., Parks, D.H., Fischer, W.W., Hugenholtz, P., 2017. On the origins of oxygenic photosynthesis and aerobic respiration in Cyanobacteria. Science 355, 1436–1440.

van Zuilen, M.A., Fliegel, D., Wirth, R., Lepland, A., Qu, Y., Schreiber, A., Romashkin, A.E., Philippot, P., 2012. Mineral-templated growth of natural graphite films. Geochim. Cosmochim. Acta 83, 252–262.

Wacey, D., Menon, S., Green, L., Gerstmann, D., Kong, C., Mcloughlin, N., Saunders, M., Brasier, M., 2012. Taphonomy of very ancient microfossils from the ~3400 Ma Strelley Pool Formation and ~1900 Ma Gunflint Formation: new insights using a focused ion beam. Precambr. Res. 220–221, 234–250.

Williford, K.H., Ushikubo, T., Schopf, J.W., Lepot, K., Kitajima, K., Valley, J.W., 2013. Preservation and detection of microstructural and taxonomic correlations in the carbon isotopic compositions of individual Precambrian microfossils. Geochim. Cosmochim. Acta 104, 165–182.

Xu, Z.L., Awramik, S.M., 2002. The Gaoyuzhuang palaeobiology. Acta Bot. Sin. 44, 617–627.

Zhang, Y., 1981. Proterozoic stromatolite microfloras of the Gaoyuzhuang Formation (Early Sinian; Riphean), Hebei, China. J. Paleontol. 55, 485–506.